

# Argon, neon, and nitrogen impurity transport in the edge and SOL regions of a Tokamak

Shrish Raj, N Bisai, Vijay Shankar, and A Sen

*Institute for Plasma Research, A CI of Homi Bhabha National Institute, Bhat, Gandhinagar, Gujarat, India-382428*

Numerical simulations of the interchange plasma turbulence in the presence of medium-Z impurities ( $N_2$ ,  $Ne$ ,  $Ar$ ) seeding have been performed using BOUT++. These simulation results are used to study the impurity transport mechanism in the edge and scrape-off layer (SOL) regions. An analytical relation for the impurity ion density with the vorticity, sources and sinks, and mass to charge ratio has also been derived. Simulation shows that  $Ar^+$  moves more strongly inward compared to  $N^+$  and  $Ne^+$  that has been verified from the analytical relation. The most abundant species move both in the inward and outward directions, but on average they mainly move outward. These behaviors have been confirmed using cross-correlation techniques. The inward transport or negative flux of the impurity ions is found directly associated with the monopolar density holes in the presence of the electron temperature gradient whereas the outward transport is associated with the plasma blobs. The inward impurity transport has been analyzed using hole fraction analysis.  $\sim 44\%$  of  $Ar^+$ ,  $\sim 28\%$  of  $Ne^+$ , and  $\sim 25\%$  of  $N^+$  ions of their total impurity densities are transported inward mainly through the avalanche events of the turbulent plasma.

## I. INTRODUCTION

The anomalous plasma transport in the edge and scrape-off layer (SOL) regions gives rise to large particle and heat loads on the plasma facing material plates in tokamaks or stellarators. These loads can damage the material plates and hence become a potential threat to the safe operation of the machines. Therefore, these situations demand a controlling mechanism so that these loads can be reduced within a safe operating limit. The medium-Z impurities such as nitrogen ( $N_2$ ), neon ( $Ne$ ), and argon ( $Ar$ ) gases are found effective in controlling the heat and particle fluxes in the boundary region of the tokamaks [1–8]. These gases and ions radiate and convert a major portion of energy into radiation [9]. The studies in references [4, 5, 8] have indicated about 40%-50% mitigation of the peak heat loads on the divertor plates. A comparative study presented in ref.[6] suggests that neon is found to radiate more efficiently on closed field lines than nitrogen. From ref.[7] it has been found that if the seeding rate exceeds a certain threshold for a given particle and heat load crossing the separatrix then an inward pinch is triggered which is mainly related to the reduction in the edge localized modes (ELM) activities. Also, these impurities may play an important role to detach the plasma from the material walls so that the direct heat and particle loads can be reduced on these material plates; detailed detachment physics has been reported in refs. [9–15]. However these impurity ions move inside the magnetic device and radiate, hence, the inner plasma near the core cools down [16–19]. This is an undesirable situation - could be avoided if the inward transport of the impurity ions is controlled. For this purpose, we need to know the exact physical mechanisms for the inward transport of the impurity ions.

The tokamak plasma has high levels of density

fluctuations in the edge and SOL regions mainly due to the interchange/drift wave instabilities [20–23]. These unstable modes make the plasma into a high turbulence states that generate a type of coherent structure known as “blob” where the local plasma density is a few times higher than the background density. A generation of the plasma blob is also often associated with a generation of plasma “hole” where the plasma density is lower than the background plasma density. The blobs and holes move in the edge and SOL regions and participate in the plasma transport [10, 24–26].

The plasma turbulence is modified by impurity seeding. In particular impurity ions which are relatively heavier compared to the main plasma ions contribute more strongly to the polarization drifts that modify the plasma vorticity and hence the plasma turbulence. The modification in the plasma vorticity again modifies the impurity ion dynamics and hence in this way the plasma-impurity interaction behaves self-consistently. Numerous studies have been done experimentally [27–29] as well as numerically in past related to the plasma-impurity interaction in the boundary region of tokamaks. Authors have used a variety of numerical codes such as SOLPS-ITER [5, 30], SOLPS [4], COREDIV [7], EMC3-EIRENE [8, 31], and EDGE2D-EIRENE [6]. In the most recent works [2, 3], it has been found that the impurity ions with single or double-positive charges due to the plasma-impurity interactions move inward with a velocity of about fraction of  $c_s$  (sound speed) so that these fluxes are negative. The detailed investigations of plasma-impurity interaction shown in Ref.[32] suggest that the blobs not only carry plasma but also carry fully stripped impurity ions from the hot plasma towards the walls and the holes carry freshly ionized impurity atoms from the walls towards the hotter region. In Refs.[33], authors reported that the transport of impurity ions is associated with the plasma blobs/holes using 3D-PIC seeded blob/hole simulation. But transport

in the presence of plasma turbulence associated with finite temperature gradient was missing. The present simulation work is dedicated to the study of impurity transport associated with these blobs and holes which are generated by the interchange plasma turbulence in the edge and SOL regions of tokamak in the presence of the finite electron temperature gradient that may differ from the dipolar distribution of the impurity ions within the plasma blob/hole structures as described in Ref.[33]. For this purpose, the impurity transport studies in the presence of the nonlinear coupling between impurity and plasma turbulence have been performed using two-dimensional (2D) numerical simulations. The main emphasis has been given to the transport mechanism associated with the propagation of blobs and holes where these are generated self-consistently from the plasma turbulence. We have obtained an analytical relation between the density of these primary impurity ions and the vorticity in the presence of the impurity sources and sinks as the minimum and maximum values of the vorticity normally correspond to the blobs and holes, respectively. The analytical relation has been validated with the numerical results. It is found that the plasma vorticity is monopolar in the presence of finite electron temperature gradient [34, 35]. The first ionization species mainly move inward in the edge region near the last closed flux (LCFS) and in the SOL region, all ions move radially outward. The most abundant species in the edge region move inward and outward but on average, they move radially outward direction. It is to be noted that the temperature in the hole is low such that recombination is preferred over ionization and therefore the higher charged species present in the hole will quickly recombine to the low ionization state. But in contrast, the temperature in the blob is high enough such that ionization dominates over recombination and hence the lower charged species will quickly ionize to the higher charged states. To validate these facts we have presented the cross-correlation between the impurity ions and plasma density in the edge and SOL regions. We have also quantified the amount of impurity transport by holes in the edge and SOL regions. It has been found in the simulation that the poloidal and time-averaged density of impurity species related to plasma density holes are about 44% of  $\text{Ar}^+$ , 28% of  $\text{Ne}^+$ , and 25% of  $\text{N}^+$  of their total impurity densities which are being transported radially inward in the edge region.

The paper is organized as follows. The numerical simulation method has been described in section-II. The derivation of the analytical expression for the impurity ion density has been described in section-III. The results related to the impurity transport mechanism from 2D simulations are described in section-IV. A brief summary and some concluding remarks are given in section-V.

## II. MODEL EQUATIONS AND NUMERICAL SIMULATION

The model equations used for the simulations couple the turbulence in the edge and SOL regions with the medium-Z impurity gas dynamics. Depending on the degree of electron impact ionization and recombination rates, the impurity ions may exist in multiple charge states. The model equations consist of the electron continuity equation, quasi-neutrality relation, electron energy conservation, and conservation of the impurity ions and the neutral gas. A simple diffusive model has been used to describe impurity dynamics in the impurity conservation equation. We have assumed the ions of the main plasma and the ions of these impurities are cold. These equations have been described in refs.[2, 3] that have been used for this present simulation. Numerically, all the radial derivatives have been computed using a finite difference technique. The Neumann boundary condition (zero gradient) has been applied to the electron density, electron temperature, and density related to all ions in the radial direction. The poloidal boundary conditions are periodic for all the variables, where Fourier transformation has been used for all the variables in the poloidal direction using the fastest Fourier transformation of the west version 3 (FFTW3) routines. The time evolution of all the species has been obtained using a fourth-order Adams-Basforth method. The simulation zone has a radial size  $L_x = 128\rho_s$  and a poloidal size  $L_y = 256\rho_s$ , where  $\rho_s$  is ion gyroradius. We have used 132 modes in the radial direction and 128 Fourier modes in the poloidal direction. 132 modes in the radial direction with  $L_x = 128\rho_s$  give a grid resolution of  $\Delta x = 0.96\rho_s$ , which is about  $3.8 \times 10^{-4}$  m [2, 3]. The Poisson brackets are solved using a third-order accurate up-winding method. The potential has been solved from the vorticity using the boundary value of the potential as  $\Lambda T_e$  at the outer boundary (in SOL) and  $-T_e \ln(n)$  at the inner boundary (in edge), where  $\Lambda$  is related to the floating potential. The input parameters used in our simulations are closely related to Aditya-U Tokamak parameters in the edge and SOL regions and the other details of the model can be found in refs. [1, 3, 36]. The numerical simulations have been done using BOUT++ framework [37].

## III. ANALYTICAL ESTIMATION OF THE IMPURITY ION DENSITY WITH VORTICITY

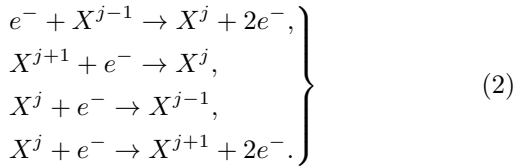
In this section, we investigate a relationship related to the impurity ion density ( $n_{imp}$ ) with the plasma vorticity, and the impurity ion sources and sinks. The equation can be written as:

$$\frac{\partial n_{imp}}{\partial t} + \vec{\nabla}_\perp \cdot (n_{imp} \vec{v}_{\perp imp}) + \nabla_\parallel (n_{imp} v_{\parallel imp}) = S_i. \quad (1)$$

$\nabla_{\perp}$  and  $\nabla_{\parallel}$  indicate the differential operators in  $(x, y)$  plane and  $z$  direction.  $t$  indicates time.  $x$  and  $y$  correspond to the radial and poloidal coordinates. The magnetic field  $\vec{B}$  acts in  $z$  direction.  $\vec{v}_{\perp imp}$  is related to  $\vec{E} \times \vec{B}$  and polarization drifts that can be written as;

$$\vec{v}_{\perp imp} = \frac{m_{imp}}{q_{imp}} \left( \frac{\partial \vec{E}}{\partial t} + (\vec{v}_E \cdot \vec{\nabla}) \vec{E} \right) + \vec{v}_E,$$

the first term is ion polarization drift and the second term is related to  $\vec{E} \times \vec{B}$  drift;  $\vec{v}_E = \vec{E} \times \vec{B}/B_0^2$ .  $\vec{E}$  represents the electric field,  $B_0$  represents the magnitude of toroidal magnetic field.  $\vec{v}_{\parallel imp} = \sqrt{\sum_i n_{imp}/nc_{s,imp}}$  where  $c_{s,imp}$  is the common sound speed of ions [38].  $n$  indicates the electron density and  $m_{imp}$  is the mass of the impurity. The ion diamagnetic term has not been taken into account because of the cold-ion approximation.  $S_i$  is the source and sink associated with the impurity ions obtained from the following chemical reactions for the impurity gas:



$X^j$  indicates impurity ions, it can be any one of  $\text{N}_2$ ,  $\text{Ne}$ , and  $\text{Ar}$  ions.  $j$  indicates charge states.  $j = 1, 2, \dots$  indicate the first ionization, second ionization states, etc. The continuity equation of  $X^j$  considering all the sources and sinks from the above reactions can be written as

$$\frac{dn_{imp}}{dt} - An_{imp} \frac{d\nabla_{\perp}^2 \phi}{dt} - n_{imp} g \frac{\partial \phi}{\partial y} = S_i - \nabla_{\parallel} \cdot (n_{imp} v_{\parallel imp}). \quad (3)$$

$A$  is the ratio of mass and charge of the impurity ions, i.e.,  $A = m_{imp}/(qj)$ .  $q$  indicates the charge of a proton. Here,  $d/dt = \partial/\partial t + \vec{v}_E \cdot \vec{\nabla}_{\perp}$ . The loss of impurity ions in the parallel direction of the magnetic field in the sheath-connected region has been taken into account. Boussinesq approximation has been taken in the second term of Eq.(3). With these approximations, Eq.(3) can be written as

$$\frac{dn_{imp}}{dt} - n_{imp} \frac{d}{dt} [A \nabla_{\perp}^2 \phi] + n_{imp} S_{l2} = S_{f2} + g \frac{\partial \phi}{\partial y} \quad (4)$$

$S_{f2}$  is the source of  $X^+$  obtained from the first two reactions as indicated in Eq.(2). It represents the rate at which the impurity ions are being formed in the simulation.  $S_{l2}$  is the effective sink related to the last two reactions as indicated in Eq.(2) including the parallel loss terms. It is to be noted that the dimension of  $S_{l2}$  is per second so that  $n_{imp} S_{l2}$  represents the loss rate of the impurity ions. Performing the time integration of Eq.(4)

we can write the impurity ion density in Lagrange frame that moves with  $\vec{E} \times \vec{B}$  drift velocity as:

$$n_{imp} = S_{eff} \exp(A \nabla_{\perp}^2 \phi) \quad (5)$$

where,

$$S_{eff} = e^{- \int S_{l2} dt} \left[ \int (e^{-A \nabla_{\perp}^2 \phi} e^{\int S_{l2} dt} S_{f2}) dt + c \right].$$

$c$  represents the integration constant. The term  $g(\partial \phi / \partial y)$  is not taken into account as  $g = c_s^2/R$ , where  $R$  is the major radius,  $c_s$  is the sound speed and its value in the dimensionless unit for ADITYA-U in the edge region is small  $g = 6.3 \times 10^{-4}$ . Equation-5 indicates that the impurity ion density is mainly governed by  $A$ , vorticity, and  $S_{eff}$  terms. We have  $A = m_{imp}/(qj)$ , consequently the magnitude of  $n_{imp}$  will be lower for higher ionization species than the lower ionization species, which indicates that the magnitude of  $n_{imp}$  for the higher ionization species drops exponentially for a given  $S_{eff}$  and  $\nabla_{\perp}^2 \phi$ . It is to be noted that in the absence of  $S_{f2}$  and  $S_{l2}$  Eq.(5) corresponds to  $S_{eff} = c$  that gives

$$n_{imp} = c \exp(A \nabla_{\perp}^2 \phi).$$

Here,  $c$  corresponds to the impurity ion density. This is the case as derived by Hasegawa and Ishiguro in ref.[33] where they showed that impurity ion density depends on the vorticity of the plasma. A double peak of impurity ion density has been observed within a plasma hole in their simulations [33] as the electron temperature was assumed uniform. But in our case, we have used finite  $T_e$  gradient in the model equation that may give a monopolar vorticity [34, 35]. The presence of finite electron temperature in the edge region, the potential can be written as  $\phi = \langle T_e \log(n) \rangle$ . As  $T_e$  and  $\log(n)$  will be maximum/minimum at the center of the blob/hole, this will give a maximum/minimum of  $\phi$  at the center of a plasma blob/hole. The above relation indicates  $\phi$  will be a function of the radius (local) of the blobs and holes. Again, in the SOL region,  $\phi$  is related with  $T_e$  as  $\phi = \Lambda \langle T_e \rangle$ . The local radial electric field ( $E_x = -\partial \phi / \partial x$ ) of the blob/hole in the edge and SOL regions will give rise to spin/rotation in the direction of the local blob-axis (in the direction of the toroidal magnetic field) that will create a vortex structure. Therefore, the blob/hole structures will be associated with the vortex. Numerically, the validation of Eq.(5) has been given in the Appendix using numerical data.

#### IV. SIMULATION RESULTS

Simulation data related to impurity transport will be presented here in the statistically stationary phase of the turbulence. The equilibrium profiles of the few impurity ions, radial electric field, and radial electric field shear are shown in Fig.1(a)-(d) as these profiles play

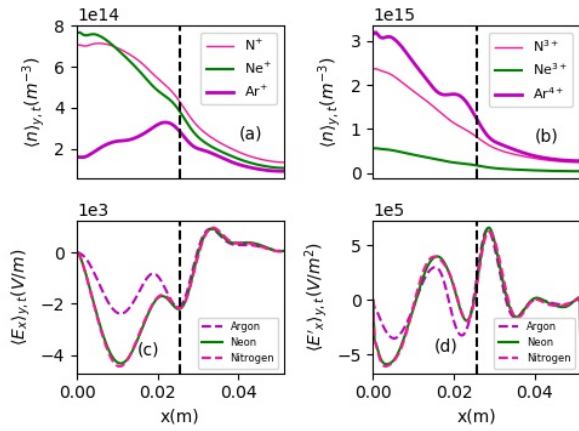


Figure 1. (a) Radial distribution of singly stripped impurity ion density (a), the impurity neutrals, and the abundant ion species (b). (c) Radial variation of  $E_x$ . (d) Radial variation of  $E'_x$ . The vertical dotted line represents the position of the last closed flux surface (LCFS) and  $\langle \cdot \rangle_{y,t}$  represents long time and poloidal average.

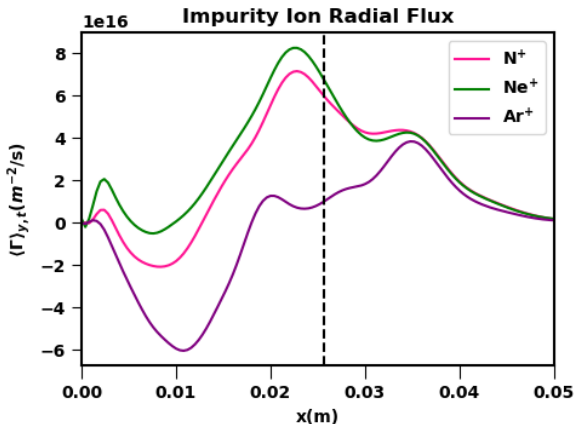


Figure 2. The radial profiles of the impurity fluxes of  $N^+$ ,  $Ne^+$ ,  $Ar^+$  ions obtained from the numerical simulation data using longtime and poloidal averages. The position of LCFS has been shown by the vertical dotted line.

an important role in the transport processes. The radial distribution of the first ionization species ( $N^+$ ,  $Ne^+$ ,  $Ar^+$ ) has been shown in Fig.1(a). It shows that  $N^+$ , and  $Ne^+$  ions densities are maximum in the edge region near  $x \sim 0.01$  m whereas  $Ar^+$  ion density is maximum near LCFS at  $x \sim 0.025$  m. The ionization potential of Ar gas is lower than  $N_2$  and Ne gases so these gases are ionized at the higher  $T_e$  that is available at the lower values near  $x = 0.01$  m. Also the recombination rate of the higher ionization such as  $Ar^{2+}$  is higher than  $N^{2+}$  and  $Ne^{2+}$  is also playing a role in this behavior. The studies in refs.[2, 3] indicate that in the statistically stationary phase of the turbulence  $N^{3+}$ ,  $Ne^{3+}$ , and  $Ar^{4+}$  ions are the most abundant. The radial profiles

of these ions are shown in Fig.1(b). These profiles have been determined from various factors such as ionization potential, recombination cross-sections, and the interaction of the neutral gas with the turbulence as described in refs.[1–3]. The radial electric field  $E_x$  has been shown in Fig.1(c). It is found that  $E_x$  is modified in the presence of Ar gas than  $N_2$  and Ne gases mainly in the edge region. It is to be noted that the modification in  $E_x$  is related to the modification in the plasma turbulence by plasma-impurity interaction. These impurities are relatively heavier compared to the main plasma ions that contribute more strongly to the polarization drifts that modify the plasma vorticity and hence the plasma turbulence. It is to be noted that the ionization/recombination process alone cannot determine the radial profiles of the ions but also the radial electric field shear  $E'_x$  plays an important role in determining the radial profile of the impurity ions. Therefore, we have plotted the radial profile of  $E'_x$  as shown in Fig.1(d). It has been found that in the case of nitrogen and neon,  $|E'_x|$  is lower than argon. The lower shear in the case of argon ions allows the inward/outward motion more strongly than the nitrogen and neon ions. The radial profiles of the impurity fluxes of  $N^+$ ,  $Ne^+$ ,  $Ar^+$  ions obtained from the numerical simulation data have been shown in Fig.2. The flux of  $Ar^+$  is more negative than  $Ne^+$ ,  $N^+$  ions which indicates that  $Ar^+$  mainly move in the inward direction than the other two ions. The fluxes of the other higher ionization species are mainly positive which are not shown here but we will discuss more in this section.

Since the plasma particle transport is also associated with blobs and holes [32], therefore, it is desirable to analyze the impact of these impurity ions on these coherent structures present in the plasma. As the present study is dedicated to the mechanism of the impurity transport by the holes in the radially inward direction, we superposed the first ionization species of argon impurity with the plasma density in the  $(x, y)$  plane as shown in Fig.3. The inset plot zooms a small rectangular area to show the presence of  $Ar^+$  inside a density hole. It is found that  $Ar^+$  is maximum near the center of the hole. A similar phenomenon is also seen at the other radial positions near LCFS. In the SOL region, no such phenomenon is seen. Similarly, the superposition of  $Ne^+$  and  $N^+$  ion densities with the plasma density are shown in Fig.4 and Fig.5, respectively. These contour plots show that for  $Ne^+$  and  $N^+$  density is maximum at a location where the plasma density hole is present. In all three cases, no such maxima of the impurity ions are seen within the plasma holes in the SOL region. In the edge region, the heavier impurities have modified the plasma vorticity more strongly, therefore, these impurities behave in a more correlated way with the plasma vorticity that gives the highest impurity density with the holes where the vorticity is positive.

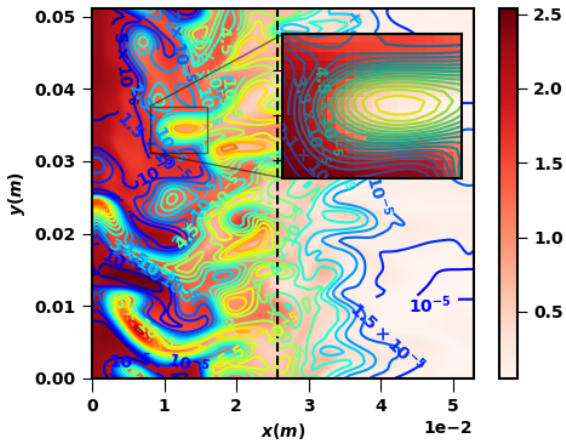


Figure 3. Superposition of 2D contour plot of Ar<sup>+</sup> with plasma density indicated by colormap ("Reds"). Ar<sup>+</sup> is maximum at the density hole near LCFS.

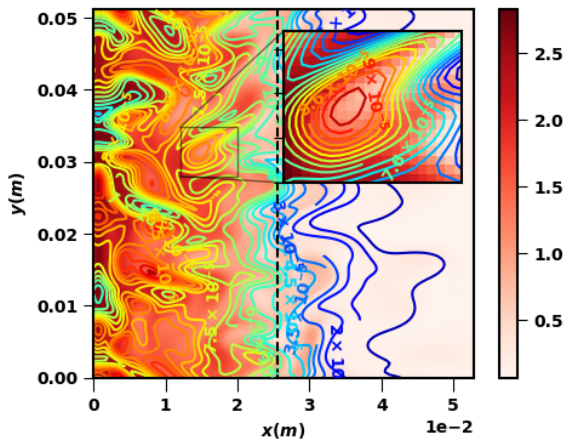


Figure 4. Superposition of Ne<sup>+</sup> (contour lines) with plasma density ("Reds", colormap). It indicates Ne<sup>+</sup> is maximum at the density hole near LCFS.

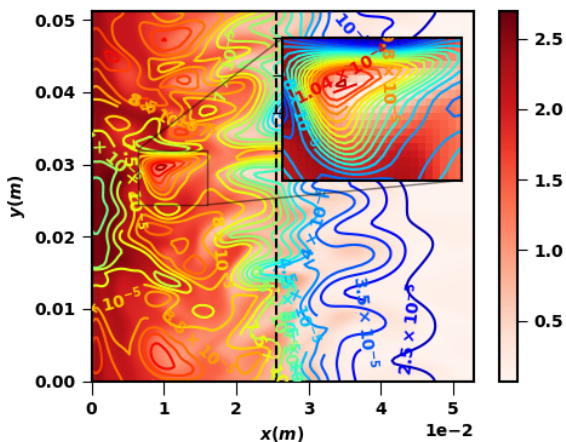


Figure 5. Superposition of contour plot of N<sup>+</sup> with plasma density indicated by colormap ("Reds"). This indicates N<sup>+</sup> is the maximum at the density hole near LCFS.

To show the simultaneous occurrence of impurity ion density maxima and plasma density holes for a large number of cases, we have presented cross-correlations between the two time series obtained from the numerical simulations related to the plasma density and the density related to the first ionization species at the four radial-poloidal (0.01m,0.025m), (0.016m,0.025m), (0.028m,0.025m), and (0.036m,0.025m) locations as shown in Fig.6. There is no definite choice of the four locations but these can help to estimate the cross-correlation in other radial locations. The negative cross-correlation coefficient primarily in the edge region for the three cases indicates that when one density increases, the other decreases. The cross-correlation coefficient has been obtained using the relation:  $C_r[\tau] = \sum_{t=0}^T s_1[t] * s_2[t - \tau]$ , where  $C_r$  is the cross-correlation coefficient for two different signals  $s_1$  and  $s_2$  obtained after taking the sum of their convolution. It is to be noted that  $\tau$  varies from 0 to  $T$ . The contour plots shown in Figs.3, 4, and 5 confirm that the impurity ion density is maximum where the plasma density is minimum (holes). Therefore, from the cross-correlation analysis and the contour plots, we can conclude that the holes are mainly associated with the maxima of the first ionization species density. The first ionization species behave slightly differently than the main plasma, therefore, the anti-correlation sustains up to a finite time, and after that they decorrelate. The simulation results indicate that when the holes move radially inward the impurity ions inside the holes also move inward so that both are correlated till the cross-correlation time that is roughly defined by the time duration when the coefficient drops to 1/e of the maximum coefficient. This happens mainly near LCFS. It is to be noted that the first ionization species inside the hole will be less probable to convert into second ionization species than the first ionization species outside the holes. The holes maintain low temperature than the background up to the auto-correlation time, therefore, these will not be ionized further or less probable to convert into the second ionization species.

The accumulation of the impurity ions with the density hole as shown in Figs.3, 4, and 5 could be explained using Eq.(5), it indicates that  $n_{imp}$  will be maximum when  $\nabla_{\perp}^2 \phi$  is maximum. The interchange plasma turbulence indicates that  $\nabla_{\perp}^2 \phi$  is positive-maximum at the hole position and negative-minimum at the blob position. Therefore,  $n_{imp}$  will be maximum (minimum) at the plasma hole (blob) location. This indicates that the impurity ion density is found to be correlated with the positive vorticity in the edge region or in other words the impurity ion density fluctuation is mainly governed by instantaneous vorticity fluctuation. We have described this behavior that is related to the first ionization species. The same phenomenon is applicable to the second ionization species but in this case  $n_{imp}$  will be lower as it depends on  $A$  where  $A$  will be

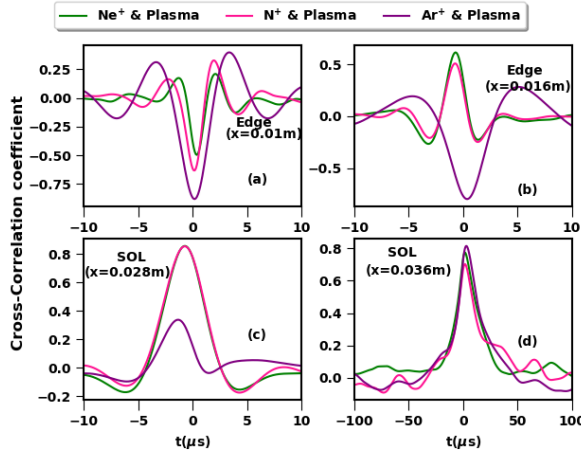


Figure 6. Radial variation of plasma density and singly stripped impurity ion density correlation.

half for the second ionization species than the first. Similarly for the third, fourth, etc, species the impurity ion density within a hole will be much lower. Fig.6(b) shows similar phenomenon as in Fig.6(a), only the cross-correlation coefficient is different. In the SOL region at  $x = 0.036m$  (Fig.6(c)), and  $x = 0.028m$  (Fig.6(d)), the cross-correlation is positive which indicates that the impurity density increases with the decrease of plasma vorticity in the time series. Therefore, one can conclude that the impurity density is maximum at the position of the plasma blob. This is quite different from the phenomena in the edge region. This may be also because of the fact that both the impurity ions and blobs move radially outward direction to facilitate the outward loss mechanism, therefore, these are correlated. They are correlated till the cross-correlation time as the impurity ions behave in a slightly different way than the main plasma ions. It is to be noted that 2D simulation result indicates that in SOL region ( $x = 0.036m$ ), the plasma holes are almost absent which indicates that the anti-correlation with the impurity ions not seen. Figs.6(a)-(d) indicate that  $N^+$  and  $Ne^+$  behave differently than  $Ar^+$  ions as  $Ar^+$  has higher polarization drift than  $N^+$  and  $Ne^+$  ions. Therefore,  $Ar^+$  behaves more strongly with the plasma vorticity than the other two ions.

The cross-correlation between the plasma density and the most abundant ion density of  $N_2$ ,  $Ne$ , and  $Ar$  has been investigated as shown in Figs.7(a)-(d). These are shown at the same locations of Figs.6(a)-(d). It is to be noted that Figs.6(a)-(b) and Figs.7(a)-(b) show the opposite behavior. The correlation coefficient is negative in Figs.6(a)-(b) but in Figs.7(a)-(b) these are positive. This behavior indicates that in the edge region, the most abundant species move radially outward direction whereas the first ionization species move inward. The high  $T_e$  at lower  $x$  ionizes the first ionization species fur-

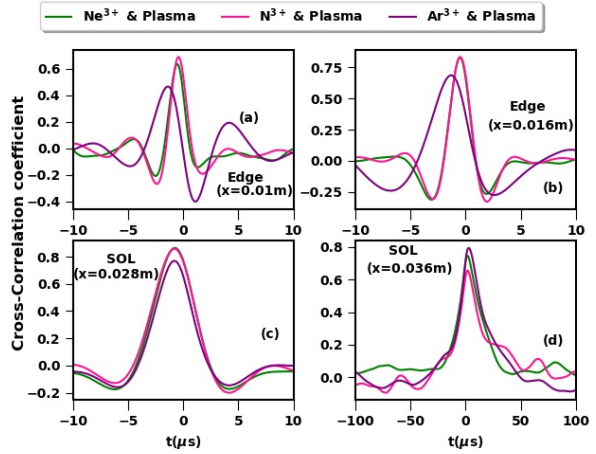


Figure 7. Radial variation of plasma density and the abundant ion species impurity ion density correlation

ther and produces the higher ionization species. These higher ionization species accumulate and the concentration builds up and when the gradient is higher than the critical gradient (when interchange instability sets in) these move radially outward due to the plasma turbulence. The blobs also move radially outward direction, therefore, both the plasma blob and the most abundant species move in the same direction which shows a positive correlation coefficient. In the edge region, a small but finite anti-correlation is observed as the holes in this region move in the inward direction with the impurity ions as explained in the previous paragraph.

The radial inward movement of the first ionization species can be calculated from Eq.(5) by estimating radial outward flux as per

$$\Gamma_{imp}^{1+} = \left\langle n_{imp} \frac{E_y}{B} \right\rangle_{t,y} \sim \left\langle S_{eff} e^{A\nabla_{\perp}^2 \phi} \frac{E_y}{B} \right\rangle_{t,y}. \quad (6)$$

Using numerical data we have estimated  $\Gamma_{imp}^{1+}$ , the results have been shown in Fig.8. The flux is negative in the edge which indicates that these ions move inward direction. The negative particle flux has been reported also in Refs.[3, 36]. It is to be noted that Eq.(6) explains the negative flux but the radial profiles as shown in Fig.6 are different from the actual numerical results as shown in Fig.2. This mismatch is mainly because we have estimated the flux in the Lagrange frame but the numerical results from the simulation have been done in the laboratory frame.

As the holes are playing a role in the impurity ion transport mainly for the first ionization species, we have investigated the hole fraction in the presence of impurity gases. The hole fraction is defined as the fraction of plasma that is contained within a hole. The low hole fraction indicates fewer numbers of plasma electrons with electron temperatures lower than the background. The radial distribution of the fraction of the plasma density in

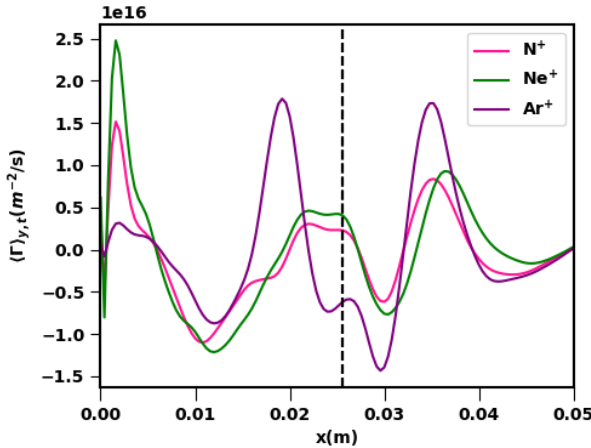


Figure 8. Comparison of the impurity ion flux using Eq.(5) where  $\nabla_{\perp}^2 \phi$  and  $S_{eff}$  have been obtained from the numerical data. The vertical dotted line indicates the position of LCFS.

the holes is shown in Fig.9. The radial distribution of the hole fraction suggests that the holes are mainly present in the edge region and there are almost no holes in the SOL region. The low electron temperature in the holes will provide a favorable condition for the inward impurity transport as the low electron temperature will lower the electron impact ionization events of the first ionization species. Therefore, the first ionization species will survive within the hole for a long time and will move much inside before reaching a high-temperature zone where the hole will be destroyed or the impurity will be ionized by the high temperature in that zone. In the case of  $\text{Ar}^+$  ions (unlike  $\text{N}^+$  and  $\text{Ne}^+$ ), the negative gradient provides stability against the interchange instability that will also favor the existence of  $\text{Ar}^+$  ions at the lower  $x$ , therefore, large numbers of  $\text{Ar}^+$  ions move in the inward direction to provide large negative impurity flux by  $\vec{E}_y \times \vec{B}$  drift.  $\vec{E}_y \times \vec{B}$  drift will be the same for both the impurity ions and main plasma particles so the structure as a whole convects in the radially inward direction. We have also estimated the percentage of impurity transport associated with the plasma density holes for all three gases from the numerical data shown in Fig.10. The conditional integration of the poloidal average of the impurity ion density is the quantification technique used in the present simulation and is represented by Eq.(7)

$$f_h = \frac{\int_0^{L_x} H n_{imp} dx}{\int_0^{L_x} n_{imp} dx}, \quad (7)$$

where  $H$  is the conditional parameter. It yields,  $H = 1$  for an event when the holes and maxima of the impurity ions exist simultaneously, otherwise  $H = 0$ . The quantity  $f_h$  gives the impurity fraction associated with the density holes.

The percentage of first ionization species associated with the holes has been shown in Fig.10. The area under

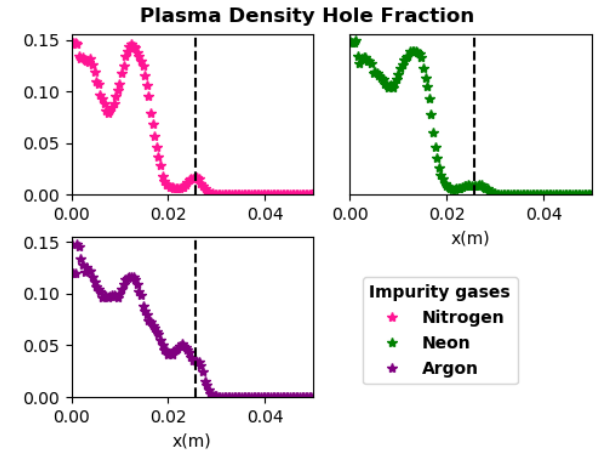


Figure 9. The plasma hole fraction in the presence of  $\text{N}_2$ ,  $\text{Ne}$ , and  $\text{Ar}$  gases. The vertical dotted lines indicate the position of LCFS.

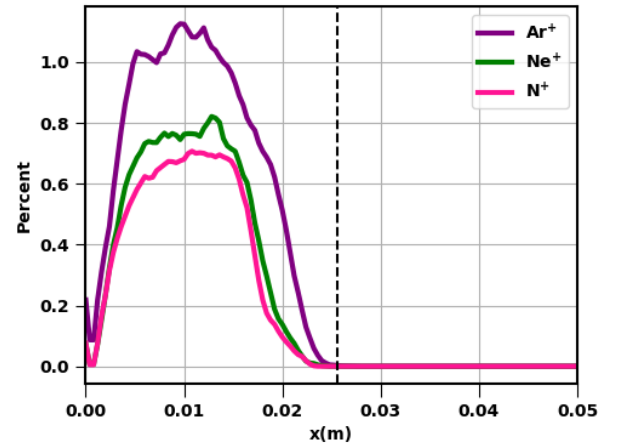


Figure 10. The fraction of impurity ions within the holes. The dotted line indicates the position of LCFS.

each curve represents the total amount of impurity ions associated with the density holes. We have calculated the area from the simulation data which gives  $\sim 44\%$  of  $\text{Ar}^+$ ,  $\sim 28\%$  of  $\text{Ne}^+$ , and  $\sim 25\%$  of  $\text{N}^+$  ions that are transported inside the edge region through the turbulent events.

## V. CONCLUSION AND DISCUSSION

Numerical simulations have performed to show the modification of the plasma turbulence by the medium-Z ( $\text{N}_2$ ,  $\text{Ne}$ , and  $\text{Ar}$ ) impurity gases in the edge and SOL regions. The main emphasis has been given to the dynamics of the impurity ions. It is found that these impurity ion motions are strongly governed by vorticity. We have derived an analytical relation for the impurity ion density with vorticity, sources and sinks, and mass-to-charge ratio.  $\text{Ar}^+$  moves more strongly inward compared to  $\text{N}^+$  and  $\text{Ne}^+$ . The most abundant species move both

in the inward and outward directions, but on an average they mainly move outward in the edge and SOL regions. We have quantified this behavior using cross-correlation techniques. The numerical simulations indicate that the impurity ions' inward transport (negative flux) is directly associated with the monopolar density holes in the presence of the electron temperature gradient. In contrast, outward transport is associated with plasma blobs. The results presented here might help in the future to understand/optimize the radiative loss in tokamak-related experiments. The inward impurity transport has been quantified using hole fraction analysis. It is found that  $\sim 44\%$  of  $\text{Ar}^+$ ,  $\sim 28\%$  of  $\text{Ne}^+$ , and  $\sim 25\%$  of  $\text{N}^+$  ions of their total impurity density that are transported inside the edge region through the intermittent events of the turbulent plasma.

## VI. ACKNOWLEDGEMENTS

The simulations are performed on the Antya cluster at the Institute for Plasma Research (IPR), India. A.S. is

thankful to the Indian National Science Academy (INSA) for its support under the INSA Senior Scientist Fellowship scheme.

## VII. APPENDIX

In order to verify the theoretical estimation of Eq.(5), we have calculated  $S_{eff}$  and  $\nabla_\perp^2 \phi$  from the numerical data as described in Section-IV and have estimated  $n_{imp}$ . Long time and poloidal averages of  $n_{imp}$  have been shown in Figure-11. These results are nearly comparable with Fig.1(a) that differ by a factor of two mainly because of the nonlinear terms but the radial variations of the profiles are almost similar. These results justify the Eq.(5).

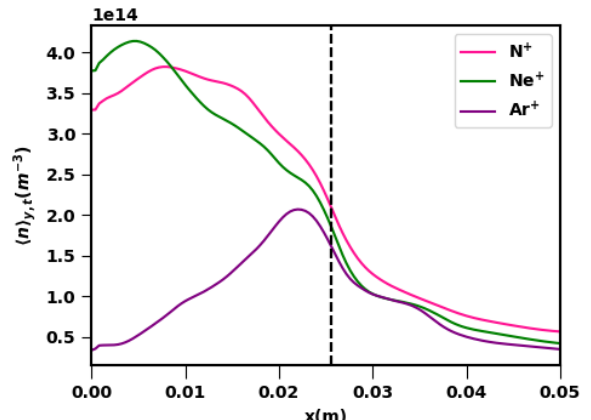


Figure 11. The radial profiles of  $n_{imp}$  as obtained from Eq.(5) and from the numerical simulation data. The vertical dotted line shows the position of LCFS.

---

[1] N Bisai, MB Chowdhuri, S Banerjee, Harshita Raj, Ritu Dey, RL Tanna, R Manchanda, KA Jadeja, J Ghosh, and Aditya Team. Dynamics of neon ions after neon gas seeding into tokamak plasma. *Nuclear Fusion*, 59(12):126013, 2019.

[2] Shrish Raj, N. Bisai, Vijay Shankar, and A. Sen. Effects of nitrogen seeding in a tokamak plasma. *Physics of Plasmas*, 27(12):122302, December 2020.

[3] Shrish Raj, N Bisai, Vijay Shankar, A Sen, Joydeep Ghosh, RL Tanna, Malay B Chowdhuri, KA Jadeja, Kumudni Assudani, and Tanmay Martin Macwan *et al.* Macwan. Studies on impurity seeding and transport in edge and SOL of tokamak plasma. *Nuclear Fusion*, 62(3):036001, 2022.

[4] Daoyuan Liu, Chaofeng Sang, Liang Wang, and Dezhen Wang. The impact of neon-seeding location on the divertor plasma in EAST. *Fusion Engineering and Design*, 136:324–329, 2018.

[5] Guozhang Jia, Xiaoju Liu, Guosheng Xu, Liang Wang, Sizheng Zhu, Hai Xie, Hang Si, Chaofeng Sang, Zhongshi Yang, Jichan Xu, *et al.* Simulations of Ar seeding by SOLPS-ITER for a slot-type divertor concept. *Physics of Plasmas*, 27(6):062509, 2020.

[6] J. Simpson, D. Moulton, C. Giroud, M. Groth, G. Corrigan, and JET Contributors. Using EDGE2D-EIRENE to simulate the effect of impurity seeding and fueling on the upstream electron separatrix temperature. *Nuclear Materials and Energy*, 20:100599, 2019.

[7] G. Telesca, I. Ivanova-Stanik, R. Zagórski, S. Brezinsek, A. Czarnecka, P. Drewelow, C. Giroud, A. Huber, S. Wiesen, M. Wischmeier, and JET contributors. High power neon seeded JET discharges: Experiments and simulations. *Nuclear Materials and Energy*, 12:882–886, 2017.

[8] F. Effenberg, Y. Feng, O. Schmitz, H. Frerichs, SA Bozhenkov, H. Hölbe, R. König, M. Krychowiak, T. Sunn Pedersen, D. Reiter, *et al.* Numerical investigation of plasma edge transport and limiter heat fluxes in wendelstein 7-x startup plasmas with EMC3-EIRENE. *Nuclear Fusion*, 57(3):036021, 2017.

[9] A. Kallenbach, M. Bernert, R. Dux, L. Casali, T. Eich, L. Giannone, A. Herrmann, R. McDermott, A. Mlynek, H. W. Müller, F. Reimold, J. Schweinzer, M. Sertoli, G. Tardini, W. Treutterer, E. Viezzier, R. Wenninger, and M. Wischmeier and. *Plasma Physics and Controlled Fusion*, 55(12):124041, 2013.

[10] Krasheninnikov S. I. and Kukushkin A. S. *Journal of Plasma Physics*, 83(5):155830501, 2017.

[11] Yanjie Zhang, Chaofeng Sang, Jiaxian Li, Guoyao Zheng, Ilya Y Senichenkov, Vladimir A Rozhansky, Chen Zhang, Yilin Wang, Xuele Zhao, and Dezhen Wang. Modeling of the effects of impurity seeding on plasma detachment and impurity screening of snowflake divertor on HL-2M tokamak by SOLPS-ITER. *Nuclear Fusion*, 62(10):106006, 2022.

[12] DP Coster. Detachment physics in SOLPS simulations. *Journal of nuclear materials*, 415(1):S545–S548, 2011.

[13] O Février, C. Theiler, J. R. Harrison, C. K. Tsui, K. Verhaegh, C Wüthrich, J. A. Boedo, H. De Oliveira, B. P. Duval, B. Labit, B. Lipschultz, R. Maurizio, H. Reimerdes, the TCV Team, and the EUROfusion MST1 Team. *Plasma. Phys. Contr. Fusion*, **62**:035017, 2020.

[14] J. R. Harrison, C. Theiler, O Février, H. de Oliveira, R. Maurizio, K. Verhaegh, A. Perek, A. Karpushov, B. Lipschultz, B. P. Duval, X. Feng, S. Henderson, B. Labit, B. Linehan, A. Merle, H. Reimerdes, U. Sheikh, C. K. Tsui, W. A. J. Vijvers, C Wüthrich, the TCV team, and the EUROfusion MST1 team. *Plasma. Phys. Contr. Fusion*, **61**:065024, 2019.

[15] J.B. Liu, L. Wang, H.Y. Guo, H.Q. Wang, G.S. Xuand F. Ding, J.C. Xu, X.J. Liu, Q.P. Yuan, K. Wu, S.C. Liu, C.F. Sang, L.Y. Meng, W. Feng, A. Hyatt, A.W. Leonard, D. Thomas, T. Zhang, T.F. Zhou, B.J. Xiao, X.Z. Gong, J. Li, B.N. Wan, and the EAST Team. *Nucl. Fusion*, **59**:126046, 2019.

[16] Albert Mollén, István Puszta, Tünde Fülöp, and Sara Moradi. Impurity transport in trapped electron mode driven turbulence. *Physics of Plasmas*, 20(3):032310, 2013.

[17] A Yu Pigarov, SI Krasheninnikov, TD Rognlien, WP West, B LaBombard, B Lipschultz, R Maingi, and V Soukhanovskii. Multi-fluid code simulations including anomalous non-diffusive transport of plasma and impurities in the tokamak SOL. *Contributions to Plasma Physics*, 44(1-3):228–234, 2004.

[18] A Yu Pigarov, EM Hollmann, SI Krasheninnikov, TD Rognlien, and WP West. Multi-ion fluid simulation of tokamak edge plasmas including non-diffusive anomalous cross-field transport. *Journal of nuclear materials*, 337:371–375, 2005.

[19] M Priego, OE Garcia, V Naulin, and J Juul Rasmussen. Anomalous diffusion, clustering, and pinch of impurities in plasma edge turbulence. *Physics of plasmas*, 12(6):062312, 2005.

[20] Y. Sarazin and Ph. Ghendrih. Intermittent particle transport in two-dimensional edge turbulence. *Physics of Plasmas*, 5(12):4214–4228, December 1998.

[21] Nirmal Bisai, Amita Das, Shishir Deshpande, Ratneshwar Jha, Predhiman Kaw, Abhijit Sen, and Raghavendra Singh. *Phys. Plasmas*, **11**:4018, 2004.

[22] D. A. D’Ippolito, J. R. Myra, and S. J. Zewben. *Phys. Plasmas*, **18**:060501, 2011.

[23] O.E. Garcia, V. Naulin, A. H. Nielsen, and Juul Rasmussen. *Phys. Rev. Lett.*, **92**:165003, 2004.

[24] Sergei I Krasheninnikov. On scrape off layer plasma transport. *Physics Letters A*, 283(5-6):368–370, 2001.

[25] N. Bisai, A. Das, S. Deshpande, R. Jha, P. Kaw, A. Sen, and R. Singh. *Phys. Plasmas*, **12**:102515, 2005.

[26] Nirmal Bisai, Amita Das, Shishir Deshpande, Ratneshwar Jha, Predhiman Kaw, Abhijit Sen, and Raghavendra Singh. *Phys. Plasmas*, **12**:072520, 2005.

[27] H.Q. Wang, H.Y. Guo, T.W. Petrie, A.W. Leonard, D.M. Thomas, J.G. Watkins, and DIII-D team. *Nuclear Materials and Energy*, **12**:942–947, 2017.

[28] T. Barbui, F. Effenberg, R. König, M. Krychowiak, O. Schmitz, J. Baldzuhn, B.D. Blackwell, B. Butten schön, P. Drews, M. Jakubowski, S. Kwak, Y. Liang, S. Liu, H. Niemann, T. Sunn Pedersen, J. Svensson, D. Zhang, and the W7-X Team. *Nucl. Fusion*, **59**:076008, 2019.

[29] H. Tanaka, G. Kawamura, S. Masuzaki, M. Kobayashi, T. Akiyama, B.J. Peterson, K. Mukai, R. Sano, S.Y. Dai, R. Sakamoto, T. Morisaki, N. Ohno, and LHD Experiment Group. *Nuclear Materials and Energy*, **12**:241–246, 2017.

[30] Rong Wang, Zhongshi Yang, Kedong Li, Guosheng Xu, Guozhang Jia, Guojian Niu, Feifei Nian, Tao He, Lingyi Meng, Xin Lin, et al. Modeling of the impact of NEON seeding on the detachment in east by SOLPS-ITER. *Physics of Plasmas*, 29(11):112502, 2022.

[31] G Kawamura, H Tanaka, K Mukai, B Peterson, S Y Dai, S Masuzaki, M Kobayashi, Y Suzuki, Y Feng, and LHD Experiment Group. *Plasma. Phys. Contr. Fusion*, **60**:084005, 2018.

[32] SI Krasheninnikov, DA D’ippolito, and JR Myra. Recent theoretical progress in understanding coherent structures in edge and SOL turbulence. *Journal of Plasma Physics*, 74(5):679–717, 2008.

[33] Hiroki Hasegawa and Seiji Ishiguro. Impurity transport caused by blob and hole propagations. *Nuclear Fusion*, 57(11):116008, 2017.

[34] N. Bisai and P. K. Kaw. *Phys. Plasmas*, **20**:042509, 2013.

[35] Vijay Shankar, Nirmal Bisai, Shrish Raj, and Abhijit Sen. Finite electron temperature gradient effects on blob formation in the scrape-off layer of a tokamak plasma. *Nuclear Fusion*, 61(6):066008, 2021.

[36] Harshita Raj, Tanmay Macwan, Kaushalender Singh, Suman Dolui, Joydeep Ghosh, Nirmal K Bisai, KA Jadeja, KM Patel, NC Patel, RL Tanna, et al. Effect of periodic gas-puffs on drift-tearing modes in ADITYA/ADITYA-U tokamak discharges. *Nuclear Fusion*, 60(3):036012, 2020.

[37] B. D. Dudson, X. Q. Xu, M. V. Umansky, H. R. Wilson, and P. B. Snyder. *Plasma. Phys. Contr. Fusion*, **53**:054005, 2011.

[38] S D Baalrud and C C Hegna. *Phys. Plasmas*, **18**:023505, 2011.